Journal of Atmospheric and Solar–Terrestrial Physics 212 (2021) 105506

Contents lists available at ScienceDirect

Journal of Atmospheric and Solar-Terrestrial Physics

journal homepage: www.elsevier.com/locate/jastp

Research Paper

Long-term trend and solar cycle in the middle atmosphere temperature revealed from merged HALOE and SABER datasets

Tao Li [a], Jia Yue [b,c,*], James M. Russell III [d], Xi Zhang [a]

[a] Department of Earth and Planetary Sciences, University of California, Santa Cruz, CA, USA
[b] Catholic University of America, DC, USA
[c] NASA Goddard Space Flight Center, MD, USA
[d] Hampton University, Hampton, VA, USA

A R T I C L E I N F O

Keywords:
Temperature
Long term trend
Solar cycle
Stratosphere and mesosphere

A B S T R A C T

The middle atmosphere temperature trend and solar cycle have been studied with long-term ground-based and satellite datasets and/or model simulations. Single satellite observations for middle atmosphere temperature are not long enough (less than 2 solar cycles) to derive long-term trend and solar cycle effects with great confidence. Using a nearly 30-year dataset merged from the Halogen Occultation Experiment (HALOE) observations between 1991 and 2005 and the Sounding of the Atmosphere using Broadband Emission Radiometry (SABER) observations between 2002 and 2019, we study the long-term trend and solar cycle in the middle atmosphere temperature between 45°S and 45°N. The cooling trend is significant below 75 km with a maximum value of ~ -1.2 K/decade near 60–70 km in the southern hemisphere (SH) tropical and subtropical region. The SH cooling trend is larger than its counterpart in the northern hemisphere (NH). The trend derived from the SABER only dataset is ~1.5 times smaller than that derived from the merged dataset, which is consistent with the upper stratospheric ozone recovery after 1995. The positive temperature response to the 11-year solar cycle is ~1 K/100 solar flux units (sfu) in the upper stratosphere and lower mesosphere and increase to more than 2 K/100 sfu in the upper mesosphere of the middle latitudes. The temperature responses show clear hemispheric asymmetry with stronger responses below 70 km but weaker above in the SH than those in the NH. This is likely related to hemispheric asymmetry of wave activities induced by indirect solar radiation.

1. Introduction

Global climate change in the middle atmosphere is largely controlled by increasing greenhouse gases, e.g. CO_2, CH_4 etc. due to human activities (Beig et al., 2003) and natural variability due to the 11-year solar cycle. The increases of greenhouse gases, especially CO_2 in the atmosphere cause not only global warming in the troposphere, but also global cooling in the middle atmosphere (Roble and Dickinson, 1989). The ozone depletion in the lower stratosphere may also contribute to middle atmosphere cooling (Ramaswamy et al., 2001). Early ground-based lidar observations suggest significant cooling as large as -2-3 K/decade at middle latitudes, and as small as −0.5 K/decade in the subtropics in the stratosphere and mesosphere (Keckhut et al., 2001; Li et al., 2011). Satellite observations also reveal a cooling trend of 0.5–1.5 K/decade in the middle and upper stratosphere (Randel et al., 2009). The different types of observations and observational periods could lead to large variability of a few K/decade in the derived middle atmosphere temperature trend (Beig et al., 2003).

The long-term observational temperature datasets are extremely valuable for studying the long-term temperature trend and temperature response to the 11-year solar cycle. However, without properly and completely separating the solar cycle signal, the derived middle atmosphere temperature trend could be significantly biased (Beig, 2011a). As such, a long-term dataset covering at least 2 solar cycles is necessary to minimize the effect of decade variability on the trend. Using 14-year observations of middle atmosphere temperature by the Halogen Occultation Experiment (HALOE) onboard the Upper Atmosphere Research Satellite (UARS), Remsberg (2009) found clear negative temperature trends and positive temperature responses to 11-year solar cycle in the upper stratosphere and mesosphere between 40°S and 40°N. A recent model simulation of the middle atmosphere trend with the Whole Atmosphere Community Climate Model (WACCM) suggest good

* Corresponding author. Catholic University of America, DC, USA.
E-mail address: jia.yue@nasa.gov (J. Yue).

https://doi.org/10.1016/j.jastp.2020.105506
Received 21 August 2020; Received in revised form 28 October 2020; Accepted 9 November 2020
Available online 9 December 2020
1364-6826/

agreement with the observations of the Sounding of the Atmosphere using Broadband Emission Radiometry (SABER) instrument onboard the Thermosphere Ionosphere and Mesosphere Electric Dynamics (TIMED) satellite (Garcia et al., 2019). (Gan et al. (2017)) also found that zonal mean temperature responses to the 11-year solar cycle agree well between SABER observation and the Canadian Middle Atmosphere Model simulation.

Both HALOE and SABER observations alone are not long enough (less than 2 solar cycles) to derive either the trend or solar cycle with great confidence. Fortunately, these two satellite observations have an overlap period between 2002 and 2005, which allows us to merge 2 datasets to form a nearly 30-year global middle atmosphere temperature dataset. In this paper, we use this merged dataset to derive the middle atmosphere temperature trend and temperature responses to the 11-year solar cycle from 45°S to 45°N. The data merge and multivariate linear regression analysis methods are described in section 2. Section 3 presents the results of the derived temperature trend and Section 3 presents solar cycle results, followed by a brief summary in section 5.

2. Data merge and analysis method

The HALOE instrument onboard the UARS satellite (Russell et al., 1993) has used solar occultation to measure the transmission of the CO_2 2.8 μm band during sunset (SS) and sunrise (SR) that are ~10–14 local hours apart and retrieve the vertical profiles of middle atmosphere temperature from October 1991 until November 2005. The observations were mostly made between 50°S and 50°N with missing data near 40°–50° in the summer hemisphere (Remsberg, 2008). We use the version 19 HALOE temperature dataset available at http://haloe.gats-inc.com/. The vertical resolution of the temperature profile is ~4 km and the typical measurement uncertainties are ~5 K below 80 km (Hervig et al., 1996). We first rebin all profiles to form a standard grid between 40 and 80 km with a 2 km interval and from 45°S to 45°N with a 5° latitude bin, and then calculate monthly mean profiles by averaging all available profiles within that month for SS and SR. The monthly means of SS and SR are then averaged to largely reduce diurnal tidal effects on the means and finally form a monthly mean time series for HALOE. The average of SS and SR cannot remove the semidiurnal tide effect. If only a SS or SR monthly mean is available for that month, an offset of <2 K computed from the average difference between SS and SR over the whole period is adjusted.

The SABER onboard the TIMED satellite (Russell et al., 1999) has measured middle atmosphere temperature using limb sounding of CO_2 15 μm infrared emission since January 2002. We use the version 2.0 SABER temperature datasets between 2002 and 2019 available at http://saber.gats-inc.com/. The TIMED satellite is in a near sun-synchronize orbit and has ~15 orbits a day with ~10-h difference between descending and ascending nodes. It also takes ~60 days to cover nearly 22hr local time observations. We note here that the SABER emission measurements yield many more data points than HALOE solar occultation measurements. The uncertainty for the SABER temperature measurements is less than 2K between the stratosphere and middle mesosphere with ~2 km vertical resolution. (Remsberg et al., 2008). We first obtain the daily mean temperature for both ascending and descending measurements in the same latitude and altitude bins as HALOE. To remove monthly mean diurnal tide effects, we average all available daily mean SABER profiles within a 2-month window forward sliding for 1 month to form monthly mean time series. Note that due to the samplings of the two datasets, semidiurnal tides are largely removed from the SABER monthly means, while remain in the HALOE monthly means. This could cause a bias in HALOE temperature trend if semidiurnal tides have long term changes.

To merge the two datasets of monthly mean time series, we adopt the simple mean method similar to that was used by Froidevaux et al. (2015), as $M(i) = 0.5(Y_1(i) + Y_2(i))$, Where i is individual month, and M, Y_1 and Y_2 represents merged HALOE and SABER data points respectively. Prior to the merge process, the whole HALOE and SABER data points at each latitude and altitude are offset with half of averaged differences between the two time series within the overlap period 2002–2005. Fig. 1 shows these averaged differences with SABER data points minus HALOE data points. We clearly see that the SABER monthly mean temperatures are generally 1–3K lower than HALOE temperatures below ~66 km, but 2–4K higher above. This is likely due to different sample and retrieval methods. Fig. 2 shows the monthly mean time series of HALOE (blue), SABER (red), and merged (black) at 40°N and 78 km during (a) 2002–2005 overlap period and (b) 1991–2019. It is clear that the SABER observed temperatures at this altitude and latitude are higher than HALOE temperatures (Fig. 2a). The time series in Fig. 2b shows a clear annual variation and cooling trend during the whole period.

To derive the linear trend and solar cycle from the merged dataset, we first remove the seasonal cycles by subtracting the composite monthly mean from the individual monthly mean at each altitude and latitude, and then apply a multivariate linear regression (MLR) analysis on the deseasonalized anomalies with a linear trend term, 11-year solar cycle (F10.7 cm solar flux), El Niño-Southern Oscillation (N3.4 index), Quasi-Biennial Oscillation (two orthogonal time series derived from equatorial stratospheric zonal winds), and stratospheric aerosol optical depth representing the impact of volcanic eruption. The MLR analysis method has been discussed in detail in Li et al. (2008; 2013). The 95% confidence level for each coefficient is estimated from the fitting uncertainty to be ~1.96σ (σ is the standard deviation). Fig. 3 shows the deseasonalized time series (black stars) at 40°N and 78 km, and its corresponding MLR fitting curve (blue line). The MLR fitting curve agrees well with the deseasonalized time series, and the peaks near 1992, 2002, and 2014 suggest that the solar cycle dominates the long-term variation. The Pinatubo volcanic eruption in 1991 can also cause mesosphere warming and extend to more than 2 years (She et al., 2015), which may impact the trend and solar cycle fitting. As such, we tested the MLR fitting without the index for stratospheric aerosol optical depth but removing 1991–1993 data, and the results of trend and solar cycle do not significantly change (not shown).

3. Temperature trend

Fig. 4 shows the temperature trend at 40–80 km from 45°S to 45°N derived from the HALOE and SABER merged dataset. A significant middle atmosphere cooling trend is seen throughout the region with maximum value of ~ -1.2 K/decade near 60–70 km in the tropical and

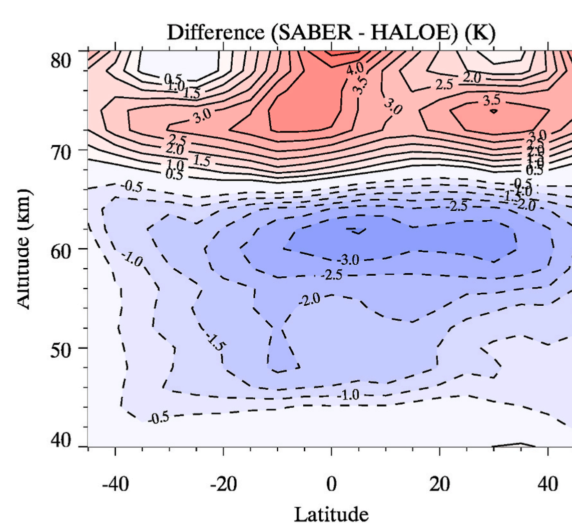

Fig. 1. Averaged differences between HALOE and SABER (SABER-HALOE) within the overlap period (2002–2005). The red color represents a positive value, while the blue color represents a negative value.

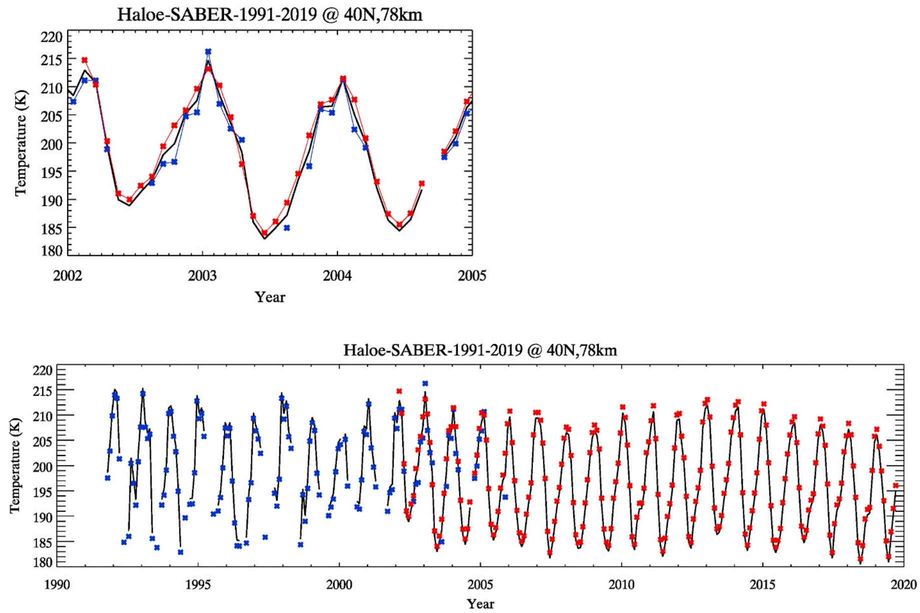

Fig. 2. Monthly mean time series of HALOE (blue), SABER (red), and merged (black) at 40N and 78 km during the 2002–2005 overlap period (a) and whole period (b).

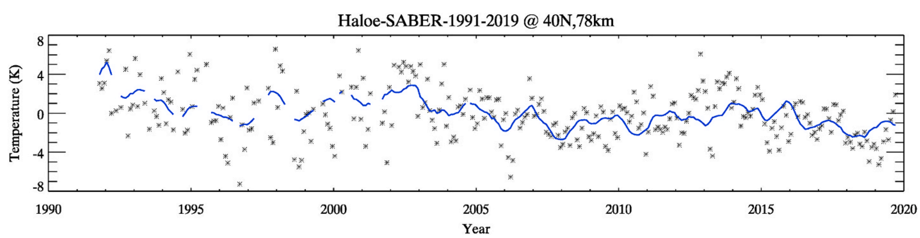

Fig. 3. Deseasonalized time series (black stars) at 40N and 78 km, and its corresponding MLR fitting curve (blue line).

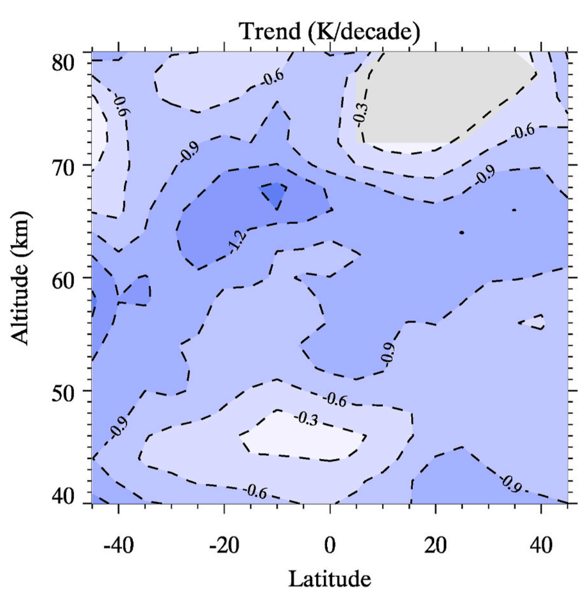

Fig. 4. Long-term temperature trend at 40–80 km from 45S to 45N derived from the merged dataset. The blue color areas represent a negative trend with contour line intervals of 0.3 K/decade. The grey areas represent the significant level below 95%.

subtropical region of Southern Hemisphere (SH). The SH cooling trend is clearly stronger than its counterpart in the Northern Hemisphere (NH). Using long-term ozone datasets observed by satellites and ozonesondes between 1997 and 2005, (Randel et al. (2007)) found that the annual mean ozone column showing decreasing trends in the SH are much larger than those in the NH. A recent Whole Atmosphere Community Climate Model (WACCM) suggest that the ozone depletion could cause a significant cooling trend in the upper stratosphere and lower mesosphere (Garcia et al., 2019). This suggests that large ozone decreasing trends in the SH may cause a larger middle atmosphere temperature cooling trends in the SH than those in the NH. We also note here that the cooling trend on the altitude levels in the middle atmosphere, especially in the mesosphere, can also be contributed by the atmosphere contraction (Akmaev et al., 2006). This effect can be ignored if the trend is measured on the pressure levels (Garcia et al., 2019).

Fig. 5 shows the differences of temperature trends derived from the merged and SABER only datasets. The cooling trends derived from the merged dataset between 1991 and 2018 are clearly 0.2–0.6 K/decade larger than those derived from the SABER only dataset between 2002 and 2018. This is consistent with the slightly increase of upper stratosphere ozone density after 1995 derived from long-term ozone lidar observations (Steinbrecht et al., 2009), which could decrease the temperature cooling trend in the middle atmosphere. The lidar observations in the Observatoire de Haute Provence, France revealed a much smaller cooling trend in the middle atmosphere after 1995 than that before 1995 (Li et al., 2011). The WACCM simulation suggests that the global averaged middle atmosphere trends are much smaller (within -1K/decade) and more uniform after 1997 than those before 1997 (∼-1.5 K/decade

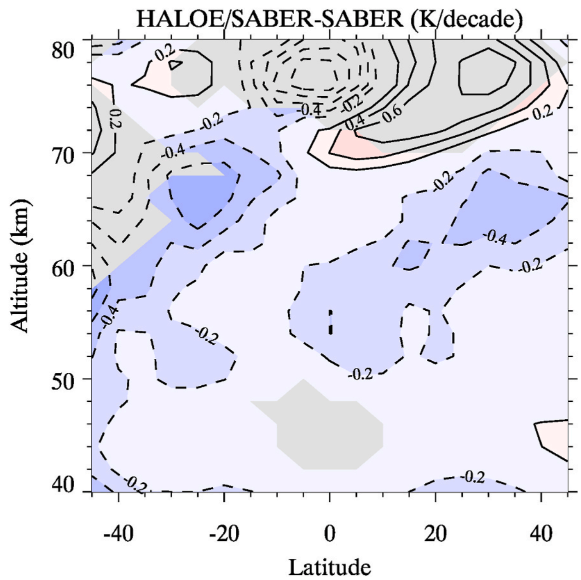

Fig. 5. Trend differences between merged and SABER only datasets. The blue color areas represent larger cooling trend derived from the merged dataset than that from SABER only. The grey areas represent the significant level below 95%.

near the stratopause) (Garcia et al., 2019). Therefore, we expect that the cooling trend derived from the merged dataset should be larger than that derived from the SABER only dataset.

To compare with long-term lidar observations, we list in Table 1 the trend comparison between merged satellite results with 1σ standard deviation and lidar results (inside the brackets) published in Li et al. (2011) and Kishore et al. (2014). These long-term (usually 10–30 years) lidar observational results are adapted from Li et al. (2011) for three NH sites at the Mauna Loa Observatory, Hawaii (MLO, 19.5°N), the Table Mountain Facility, California (TMF, 34.4°N), the Observatoire de Haute Provence, France (OHP, 43.9°N), and from Kishore et al. (2014) for one tropical site at Gadanki, India (GAD, 13.5°N) and two SH subtropical sites at Reunion Island (REU, 20.8°S) and São José dos Campos, Brazil (SJO, 23.2°S). The comparison shows qualitatively good agreement (~-1K/decade) between satellite and lidars. Some large discrepancies are usually seen in the mesosphere where lidar signal-to-noise ratios are much lower. We also note that the differences at the TMF lidar site can be as large as 3 times the mean throughout the altitude region. These differences between satellite and lidars could be due to different sampling rates and analysis methods, observational period etc. Since lidar observations are made for only a few hours per night and several nights per month, the monthly mean value will not be able to eliminate the tidal and planetary waves effect. Merged satellite datasets on the other hand average both nighttime and daytime data to eliminate the tidal and planetary effects. The long-term tidal variability can then impact the derived trend in lidar results.

Table 1
The trend comparison between merged satellite dataset results with 1σ standard deviation and lidar results (inside the brackets). The unit is K/decade.

Alt (km)	25°S (SJO, 23.2°S)	20°S (REU, 20.8°S)	15°N (GAD, 13.5°N)	20°N (MLO, 19.5°N)	35°N (TMF, 34.4°N)	45°N (OHP, 44°N)
40	−1.0 ± 0.1 (−0.3)	−0.9 ± 0.1 (−2.0)	−1.0 ± 0.1 (−1.8)	−1.0 ± 0.1 (−0.7)	−0.9 ± 0.1 (−2.5)	−1.0 ± 0.2 (−2.0)
50	−0.9 ± 0.1 (−1.3)	−0.7 ± 0.1 (−1.5)	−0.8 ± 0.1 (−0.7)	−0.8 ± 0.1 (−0.6)	−0.7 ± 0.1 (−3.0)	−0.6 ± 0.2 (−1.5)
60	−1.0 ± 0.1 (−0.4)	−1.0 ± 0.1 (−0.6)	−1.2 ± 0.1 (−2.2)	−1.3 ± 0.1 (−0.8)	−0.9 ± 0.2 (−4.5)	−0.8 ± 0.2 (−0.8)
70				−0.5 ± 0.2 (1.3)	−1.2 ± 0.2 (−4.0)	−0.8 ± 0.2 (−0.7)

4. Temperature response to 11-year solar cycle

Fig. 6 shows temperature responses to the 11-year solar cycle at 40–80 km from 45S to 45N derived from the merged dataset. The solid lines represent positive responses with the red color region representing the 95% significant level. The middle atmosphere shows a clear positive temperature response to the solar cycle between 45°S and 45°N over virtually the entire altitude range. The significant responses clearly increase in altitude from ~0.3 K/100 solar flux units (sfu) in the upper stratosphere to 1.5–2K/100 sfu in the upper mesosphere, with a maximum value of ~2.4 K/100 sfu near 80 km in the middle altitudes of both Hemispheres. The temperature responses show clear hemispheric asymmetry with stronger responses below 70 km but weaker above in the SH than those in the NH. This hemispheric asymmetry is likely related to hemispheric asymmetry of indirect solar effects on wave activities (Remsberg, 2009; Beig, 2011b).

Fig. 7 shows the differences of temperature responses to the solar cycle derived from the merged dataset and SABER only dataset. It is clear that the temperature responses derived from the merged dataset are smaller than those derived from SABER only at most of altitudes and latitudes. The differences is ~0.2 K/100 sfu in the upper stratosphere and increase to more than 1.0 K/100 sfu in the upper mesosphere, suggesting a significantly decrease of temperature response derived from the merged dataset covering 2.5 solar cycles than that derived from the dataset covering nearly 1.5 cycles. There are other long-term natural variations in temperature. The longer time series yields a more accurate fitting of the solar cycle response. Similar to the trend, we show in Table 2 the comparison between merged satellite results and lidar results published in Li et al. (2011) and Kishore et al. (2014). Most observations show positive temperature responses to the 11-year solar cycle, except lidar results at SJO for all altitudes and REU near the stratopause. The comparisons show reasonable agreement between merged satellite results and lidar results.

5. Summary

We developed the longest global middle atmosphere temperature

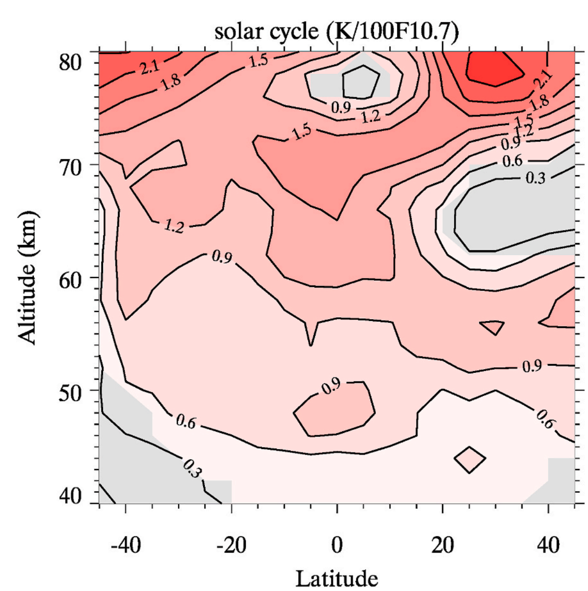

Fig. 6. Same as Fig. 4, but for solar cycle. The red color areas represent a positive solar cycle response with contour line interval of 0.3 K/100 sfu.

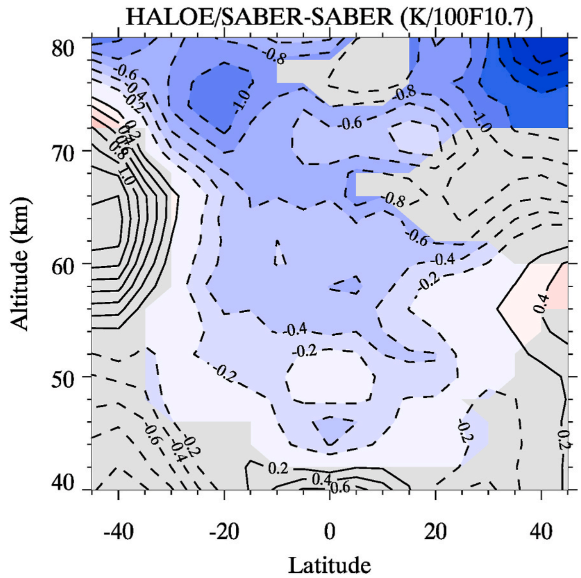

Fig. 7. Same as Fig. 5, but for solar cycle. The blue color areas represent a smaller temperature response to solar cycle derived from the merged dataset than that from SABER only.

Table 2
Same as Table 1 but for solar cycle. The unit is K/100 sfu.

Alt (km)	25°S (SJO, 23.2°S)	20°S (REU, 20.8°S)	15°N (GAD, 13.5°N)	20°N (MLO, 19.5°N)	35°N (TMF, 34.4°N)	45°N (OHP, 44°N)
40	0.2 ± 0.2 (−0.5)	0.5 ± 0.2 (0)	0.3 ± 0.2 (1.4)	0.3 ± 0.2 (0.8)	0.3 ± 0.2 (0)	0.7 ± 0.3 (−0.4)
50	0.9 ± 0.2 (−0.5)	0.7 ± 0.2 (−0.2)	0.5 ± 0.2 (0.7)	0.8 ± 0.2 (0.4)	0.6 ± 0.2 (0.2)	0.8 ± 0.3 (0.8)
60	0.7 ± 0.2 (0)	0.8 ± 0.2 (1.0)	1.2 ± 0.2 (0.8)	0.8 ± 0.2 (0.8)	0.6 ± 0.3 (0.8)	1.1 ± 0.4 (1.8)
70			1.6 ± 0.4 (0)	1.3 ± 0.4 (0.6)	0.9 ± 0.4 (2.1)	0.3 ± 0.4 (0.5)

dataset available by merging two satellite datasets observed by HALOE between 1991 and 2005 and SABER between 2002 and 2018. Using this merged dataset and multivariate linear regression analysis, we derive the middle atmosphere temperature trend and temperature response to the 11-year solar cycle from 45S to 45N between 40 and 80 km. The temperature cooling trend is significant throughout the region with a maximum cooling of −1.2 K/decade near 60–70 km in the SH tropical and subtropical region. The derived middle atmosphere cooling trends are in good agreement with those derived from various ground-based long-term lidar observations and model simulations. The cooling trends derived from the merged dataset between 1991 and 2018 are 0.2–0.6 K/decade larger than those derived from the SABER only dataset between 2002 and 2018, consistent with the slight increase of upper stratosphere ozone density after 1995.

The positive temperature responses to the 11-year solar cycle are significant between 45S and 45N in most altitude regions. The responses clearly increase in altitude from ~0.3 K/100 sfu in the upper stratosphere to 1.5–2K/100 sfu in the upper mesosphere, reaching a maximum value of ~2.4 K/100 sfu near 80 km in the middle altitudes of both Hemispheres. Temperature responses derived from the merged dataset are smaller than those derived from the SABER dataset only at most of altitudes and latitudes. Our merged, nearly 30-year, global satellite-observed dataset analysis yields reliable results showing middle atmosphere trends and temperature responses to the 11-year solar cycle and they provide constraints for future model simulations of global climate change.

Declaration of competing interest

The authors declare that they have no known competing financial interests or personal relationships that could have appeared to influence the work reported in this paper.

Acknowledgments

This work was carried out at the University of California, Santa Cruz and Hampton University, under support of the National Science Foundation grant AGS-1901126 and NASA AIM and TIMED/SABER missions. The HALOE dataset is downloaded from http://haloe.gats-inc.com/and SABER data is downloaded from http://saber.gats-inc.com/.

References

Akmaev, R.A., Fomichev, V.I., Zhu, X., 2006. Impact of middle- atmospheric composition changes on greenhouse cooling in the upper atmosphere. J. Atmos. Sol. Terr. Phys. 68, 1879–1889. https://doi.org/10.1016/j.jastp.2006.03.008.
Beig, G., et al., 2003. Review of mesospheric temperature trends. Rev. Geophys. 41.
Beig, G., 2011a. Long-term trends in the temperature of the mesosphere/lower thermosphere region: 1. Anthropogenic influences. J. Geophys. Res.: Atmos. (1984–2012) 116 (A2). https://doi.org/10.1029/2011JA016646 n/a–n/a.
Beig, G., 2011b. Long-term trends in the temperature of the mesosphere/lower thermosphere region: 2. Solar response. J. Geophys. Res.: Atmos. (1984–2012) 116 (A2). https://doi.org/10.1029/2011JA016766 n/a–n/a.
Froidevaux, L., et al., 2015. Global OZone Chemistry and Related trace gas Data records for the Stratosphere (GOZCARDS): methodology and sample results with a focus on HCl, H2O, and O3. Atmos. Chem. Phys. 15 (1), 10471–10507. https://doi.org/10.5194/acp-15-10471-2015.
Gan, Q., Du, J., Fomichev, V., Ward, W., Beagley, S., Zhang, S., Yue, J., 2017. Temperature responses to the 11-year solar cycle in the mesosphere from the 31 year (1979-2010) extended Canadian Middle Atmosphere Model simulations and a comparison with the 14 year (2002-2015) TIMED/SABER observations. J. Geophys. Res.: Space Phys. 122, 4801–4818. https://doi.org/10.1002/2016JA023564.
Garcia, R.R., Yue, J., Russell III, J.M., 2019. Middle atmosphere temperature trends in the twentieth and twenty-first centuries simulated with the whole atmosphere community climate model (WACCM). J. Geophys. Res. Sp. Phys. 124 (10), 7984–7993. https://doi.org/10.1029/2019JA026909.
Hervig, M.E., et al., 1996. Validation of temperature measurements from the halogen occultation experiment. J. Geophys. Res. Atmos. 101 (D), 10. https://doi.org/10.1029/95JD01713.
Keckhut, P., Wild, J., Gelman, M., Miller, A., Hauchecorne, A., 2001. Investigations on long-term temperature changes in the upper stratosphere using lidar data and NCEP analyses. J. Geophys. Res. Atmos. 106 (D8), 7937–7944.
Kishore, P., Venkat Ratnam, M., Velicogna, I., Sivakumar, V., Bencherif, H., Clemesha, B. R., Simonich, D.M., Batista, P.P., Beig, G., 2014. Long-term trends observed in the middle atmosphere temperatures using ground based LIDARs and satellite borne measurements. Ann. Geophys. 32 (3), 301–317. https://doi.org/10.5194/angeo-32-301-2014.
Li, T., Leblanc, T., McDermid, I.S., 2008. Interannual variations of middle atmospheric temperature as measured by the JPL lidar at Mauna Loa Observatory, Hawaii (19.5°N, 155.6°W). J. Geophys. Res. 113, D14109. https://doi.org/10.1029/2007JD009764.
Li, T., Leblanc, T., McDermid, I., Keckhut, P., Hauchecorne, A., Dou, X., 2011. Middle atmosphere temperature trend and solar cycle revealed by long-term Rayleigh lidar observations. J. Geophys. Res. 116, D00P05. https://doi.org/10.1029/2010jd015275.
Li, T., Calvo, N., Yue, J., Dou, X., Russell III, J.M., Mlynczak, M.G., She, C.-Y., Xue, X., 2013. Influence of El Niño-southern oscillation in the mesosphere. Geophys. Res. Lett. 40 (12), 3292–3296. https://doi.org/10.1002/grl.50598.
Ramaswamy, V., et al., 2001. Stratospheric temperature trends: observations and model simulations. Rev. Geophys. 39 (1), 71–122. https://doi.org/10.1029/1999RG000065.
Randel, W., et al., 2009. An update of observed stratospheric temperature trends. J. Geophys. Res. Atmos. 114, D02107 https://doi.org/10.1029/2008jd010421.
Randel, William, Park, M., Wu, F., Livesey, N, 2007. A large annual cycle in ozone above the tropical tropopause linked to the Brewer–Dobson circulation. J. Atmos. Sci. 64 (12), 4479–4488. https://doi.org/10.1175/2007JAS2409.1.
Remsberg, E.E., 2008. On the response of Halogen Occultation Experiment (HALOE) stratospheric ozone and temperature to the 11-year solar cycle forcing. J. Geophys. Res.: Atmos. (1984–2012) 113 (D22). https://doi.org/10.1029/2008JD010189.
Remsberg, E.E., et al., 2008. Assessment of the quality of the version 1.07 temperature-versus-pressure profiles of the middle atmosphere from TIMED/SABER. J. Geophys. Res. 113, D17101. https://doi.org/10.1029/2008jd010013.

Remsberg, E.E., 2009. Trends and solar cycle effects in temperature versus altitude from the Halogen Occultation Experiment for the mesosphere and upper stratosphere. J. Geophys. Res.: Atmos. (1984–2012) 114 (D12), 1501. https://doi.org/10.1029/2009JD011897.

Roble, R.G., Dickinson, R.E., 1989. How will changes in carbon dioxide and methane modify the mean structure of the mesosphere and thermosphere? Geophys. Res. Lett. 16 (12), 1441–1444. https://doi.org/10.1029/GL016i012p01441 (ISSN 0094-8276).

Russell, J.M.I., Gordley, L.L., Park, J.H., Drayson, S.R., Hesketh, W.D., Cicerone, R.J., Tuck, A.F., Frederick, J.E., Harries, J.E., Crutzen, P.J., 1993. The halogen occultation experiment. J. Geophys. Res. 98 (D6), 10. https://doi.org/10.1029/93JD00799 (ISSN 0148-0227).

Russell III, J.M., Russell, J.M., Mlynczak, M.G., Gordley, L.L., Tansock, J.J., Tansock Jr., J.J., Esplin, R.W., 1999. Overview of the SABER experiment and preliminary calibration results. In: Larar, A.M. (Ed.), Proc. SPIE, vol. 3756, pp. 277–288. https://doi.org/10.1117/12.366382, 3756.

She, C.Y., Krueger, D.A., Yuan, T., 2015. Long-term midlatitude mesopause region temperature trend deduced from quarter century (1990–2014) Na lidar observations. Ann. Geophys. 33 (3), 363–369. https://doi.org/10.5194/angeo-33-363-2015.

Steinbrecht, W., et al., 2009. Ozone and temperature trends in the upper stratosphere at five stations of the Network for the Detection of Atmospheric Composition Change. Int. J. Rem. Sens. 30 (15–16), 3875–3886. https://doi.org/10.1080/01431160902821841.

Preflight Results

Document Overview

Title: Long-term trend and solar cycle in the middle atmosphere temperature revealed from merged HALOE and SABER da
Author: Tao Li
Creator: Elsevier
Producer: Acrobat Distiller 8.1.0 (Windows)

Preflight Information

Profile: Convert to PDF/A-1b
Version: Qoppa jPDFPreflight v2020R2.01
Date: May 28, 2021 8:42:25 PM

Legend: (X) - Can NOT be fixed by PDF/A-1b conversion.
(!X) - Could be fixed by PDF/A-1b conversion. User chose to be warned in PDF/A settings.

Page 1 Results

(X) Font widths must be the same in both the font dictionary and the embedded font file.

Page 4 Results

(X) Font widths must be the same in both the font dictionary and the embedded font file.
(X) Font widths must be the same in both the font dictionary and the embedded font file.
(X) Font widths must be the same in both the font dictionary and the embedded font file.
(X) Font widths must be the same in both the font dictionary and the embedded font file.
(X) Font widths must be the same in both the font dictionary and the embedded font file.
(X) Font widths must be the same in both the font dictionary and the embedded font file.
(X) Font widths must be the same in both the font dictionary and the embedded font file.
(X) Font widths must be the same in both the font dictionary and the embedded font file.
(X) Font widths must be the same in both the font dictionary and the embedded font file.
(X) Font widths must be the same in both the font dictionary and the embedded font file.
(X) Font widths must be the same in both the font dictionary and the embedded font file.
(X) Font widths must be the same in both the font dictionary and the embedded font file.
(X) Font widths must be the same in both the font dictionary and the embedded font file.
(X) Font widths must be the same in both the font dictionary and the embedded font file.
(X) Font widths must be the same in both the font dictionary and the embedded font file.
(X) Font widths must be the same in both the font dictionary and the embedded font file.
(X) Font widths must be the same in both the font dictionary and the embedded font file.
(X) Font widths must be the same in both the font dictionary and the embedded font file.
(X) Font widths must be the same in both the font dictionary and the embedded font file.
(X) Font widths must be the same in both the font dictionary and the embedded font file.
(X) Font widths must be the same in both the font dictionary and the embedded font file. - 21 more not displayed

Page 5 Results

(X) Font widths must be the same in both the font dictionary and the embedded font file.
(X) Font widths must be the same in both the font dictionary and the embedded font file.
(X) Font widths must be the same in both the font dictionary and the embedded font file.
(X) Font widths must be the same in both the font dictionary and the embedded font file.
(X) Font widths must be the same in both the font dictionary and the embedded font file.